Journal of Scientific & Industrial Research
Vol. 83, February 2024, pp. 191-203
DOI: 10.56042/jsir.v83i2.5331

Simulative Investigation of MIMO-OFDM-FSOC System over Modified Malaga Distributed Composite Atmospheric Channel

Shivaji Sinha[1,2] & Chakresh Kumar[1]*

[1]University School of Information, Communication & Technology, Guru Gobind Singh Indraprastha University, New Delhi 110 078, India

[2]JSS Academy of Technical Education, Noida 201 301, Uttar Pradesh, India

Received 03 September 2023; revised 07 January 2024; accepted 15 January 2024

In this research work, we propose a novel design for a multiple aperture based Free-Space Optical Communication (FSOC) system where the Low Density Parity Check (LDPC)-coded, M-independent parallel Quadrature Amplitude Modulation (QAM)-OFDM multiplexed data streams are transmitted over a composite Malaga atmospheric channel by selecting any one of the switching transmission schemes: diversity, hybrid, or spatial multiplexing based on channel conditions, to yield the maximum average channel capacity while satisfying the reliable Average Bit Error Rate (ABER). In diversity switching, the coded data stream is transmitted to extract diversity gains, whereas in hybrid switching, a compromise between diversity and multiplexing gains is sought to achieve the maximum outage capacity by maintaining the reliable ABER. The performance of each switching scheme is evaluated under the power-series represented Malaga distributed composite channel which comprise of losses due to turbulence-induced fading and pointing error. In this work, a closed loop approximated mathematical expressions for the Average Channel Capacity (ACC) and ABER for each transmission mode is also derived. Apart from this, a Look-Up Table (LUT) consists of threshold Signal-to-Noise Ratio (SNR) corresponding to different channel conditions is also constructed to select the optimal switching transmission scheme. The extensive simulation results clearly demonstrate that the proposed switched mode transmission based MIMO-OFDM-FSOC system has a significant improvement in ACC compared with each stand-alone system.

Keywords: Low-density parity check, Malaga atmospheric turbulence model, Orthogonal frequency division multiplexing, Power series, Signal to noise ratio

Introduction

The growing demand for secure and high-speed wireless connections has focused a lot of interest in recent years on Free Space Optical Communication (FSOC) systems, which have a well-established literature.[1] This technology has the ability to provide point-to-point wireless infrared connections with substantial unlicensed bandwidth and ease of deployment.[2] In addition to these potential advantages, the FSOC system encounters several challenges, including atmospheric turbulence, scintillation, absorption, scattering losses, and pointing errors resulting from the FSOC transceiver configuration. Eventually, the link reliability and throughput of the FSOC communication system can be degraded due to the poor signal quality received at the receiver aperture over the time.[3] The weak to strong characteristics of atmospheric turbulence are simulated by using Lognormal and Gamma-Gamma (GG) probabilistic distribution models and are more statistically represented by the generalized Malaga distribution channel model.[4,5] In the existing literature, the received optical signal is detected at the receiver by either Subcarrier Intensity Modulation (SIM) or coherent detection or Intensity Modulated/Direct Detection (IM/DD) or non-coherent detection methods. With the advancement of high-speed digital signal processors and algorithms, the SIM detection method is preferred over the IM/DD detection method due to its support for high-speed data transmission, better BER performance, and improved receiver sensitivity under strong turbulence conditions compared to IM/DD.[6] Therefore, to achieve a higher data rate, spectral efficiency, and maximum link distance, various channel fading mitigating techniques must be implemented into the proposed FSOC system design in the presence of dynamic atmospheric conditions.

Literature Review

In the existing literature survey, the research has been widely focused on minimizing channel

*Author for Correspondence
E-mail: chakreshk@ipu.ac.in

impairments or fading due to atmospheric turbulence to attain improved FSOC system performance. Recently, the Spectral Amplitude Coded Optical Code Division Multiple Access (SAC-OCDMA) technique has been integrated into hybrid OFDM-FSOC systems to improve capacity and security using multiple 20 to 30 asynchronous users. This hybrid model compared the BER performance of the hybrid FSOC system for two modified AND (M-AND) and Single Photodiode Detection (SPD) receivers over the Gamma-Gamma fading channel and identified SPD detection as superior to the M-AND receiver.[7] Furthermore, MIMO-FSOC has greatly met increasing demands for spectral-efficiency and link dependability by employing various combining strategies such as Selection Combining (SC), Equal Gain Combining (ECG), Maximal Ratio Combining (MRC), and a high data rate MIMO-FSOC system over a log normal channel.[8,9]

Channel coding techniques have also been crucial in accounting for FSO link losses due to channel fading. To estimate pointing errors, a LDPC-coded hybrid OFDM-MIMO-FSOC system was examined over a composite EW fading channel. The Monte Carlo (MC) simulations are used to validate the system's BER performance. The obtained results showed a considerable improvement in coding gain over composite fading channels when jitter or signal beam width increased.[10] Similarly, closed-form expressions for the average BER and throughput with diversity using the EGC technique have been evaluated for the conventional, LDPC-coded (1/2 code rate) hybrid 4 × 4 MIMO-FSOC system. A Quadrature Phase Shift Keying (QPSK) modulated system has shown a high coding gain of 7.5 dB and excellent average BER performance as compared to a 16-QAM-modulated hybrid FSOC system under different weather and atmospheric turbulence conditions. However, when compared to a QPSK-based hybrid FSOC system, 16-QAM provided higher throughput.[11]

In the last few years, different conventional stochastic turbulent channel models, namely Lognormal, Gamma-Gamma, negative-exponential, Rice-Nakagami, and K-distributions models, have been extensively used in literature reviews for modelling the different atmospheric turbulence conditions. However, relatively few of them have investigated advanced channel models such as Geometric Based Stochastic Models (GBSM), mm-wave channel models, and a generalized Malaga turbulence distribution model. Moreover, the Malaga (M) distribution channel model has been used recently to model other channel models, considering both large and small fading.[12]

A typical FSOC system design based on an open loop configuration has been widely investigated in previous research work where Channel State Information (CSI) was available at the receiver side. Furthermore, a very few research studies have shown interest in the closed-loop CSI information available at the transmitter side through a feedback process that can be employed to change the transmission parameter according to the atmospheric channel. However, designing a complex, closed-loop-based adaptive FSOC transmission system in time-varying, unfavorable turbulent channels could be a viable method for improving signal quality at the receiver.[13] Furthermore, integrating the multiple spatial switching modes and their switching during adaptive transmission in a MIMO FSOC system to combat signal fading and achieve a high data rate has been proven to be an extremely challenging problem. A robust diversity and spatial multiplexing techniques-based adaptive MIMO FSOC system has been designed to combat adverse and weak turbulence conditions and to achieve the optimum through put for the targeted outage probability, respectively.[14,15] Switching between spatial multiplexing and substantial transmit diversity has been studied as an intelligent way to improve the performance of a MIMO wireless communication system with a fixed coding rate and a fixed BER. By sending the instantaneous CSI feedback to the MIMO transmitter and computing the threshold Euclidean distance at the receiver, MC simulation was used to figure out how to choose between spatial multiplexing and the transmit diversity.[16,17] Later, a FSOC system based on an adaptive transmission algorithm was proposed to optimize the spectral efficiency and average power consumption for a fixed outage probability. The instantaneous change in transmit power and modulation size in response to turbulence-induced fading CSI made the proposed system much better than that to their non-adaptive counterparts.[18]

From the different literature reviews described in the preceding section, it was clear that majority of the previous work has focused on studying Single-Input Single-Output (SISO) or MIMO-FSOC systems without including switching transmission techniques under simple statistical channel models. Only a few studies have concentrated on MIMO-FSOC systems

based on SIM modulation, especially under simple outdoor atmospheric turbulence conditions.[15,19] Hence, in this research work, a modified multiple aperture adaptive OFDM-FSOC system design is proposed to improve the link performance by taking into account the composite Malaga atmospheric channel which includes the effects of the atmospheric turbulence and pointing error. This system performance can be optimized by the appropriate selection of any of the switching transmission schemes from diversity, hybrid mode, and spatial multiplexing. The proposed system has rarely been explored for these three switching transmission schemes, to the best of the authors' knowledge.

This research work proposes the following contributions

- A modified design structure of MIMO-OFDM-FSOC system is proposed, which employs three switching transmission schemes to transmit information over complex composite turbulent atmospheric link.
- To alleviate the impacts of channel fading and hence increase system link performance, LDPC encoded and 16-QAM modulated information is distributed on OFDM symbols.
- A closed loop approximation equations are derived for the outage capacity, ABER, and Average Channel Capacity (ACC) under Malaga probability distribution.
- The proposed system performance is compared for the given threshold outage probability in terms of outage channel capacity, ABER, and pointing error.

The subsequent sections of this research paper present the mathematical modelling of the MIMO signal and the composite FSO channel. The composite FSO channel is modelled using the modified Malaga probability distribution, which is based on the power series method and the pointing error. Further, the schematic block diagram of the transmitter and receiver sub-systems of the proposed MIMO-OFDM-FSOC system based on adaptive switching techniques is also presented with their mathematical analysis in detail. Finally, the performance of the proposed system is evaluated and analyzed through simulations performed prior to the conclusion of the presented research work.

MIMO Signal Modelling

The proposed MIMO-OFDM-FSOC system consists of M transmit and N receive optical transceiver apertures with $M \leq N$ and is based on adaptive switching transmission techniques, spatial multiplexing, diversity, and hybrid techniques, respectively. In spatial switching transmission, the optical signal is expressed by $X_a = \left(x_{1,} x_{2,} \ldots\ldots\ldots x_{M,}\right)^T$ and transmitted in parallel manner through M-optical apertures to increase the data rate using simple repetition codes[20] whereas, the same coded data stream $X_b = \left(x_{1,} x_{1,} \ldots\ldots\ldots x_{1,}\right)^T$ is transmitted through M-optical apertures in diversity switching to extract the diversity gain. On the other hand, in hybrid switching, t-parallel data streams represented by $X_c = \left(x_{1,} x_{2,} \ldots\ldots\ldots x_{t,}\right)^T$ are transmitted through t repetition codes over $\frac{M}{t}$ different sets of optical apertures, considering the trade-off between multiplexing and diversity gain.

In the proposed system, Eq. (1) represents a signal model of the M-aryQAM modulated data stream (x), which consists of the in-phase and the quadrature phase components $S_I(t) = \sum_{i=-\infty}^{\infty} a_i\, g(t - iT_s)$ and $S_Q(t) = \sum_{i=-\infty}^{\infty} b_j\, g(t - jT_s)$, respectively.

$$x(t) = S_I(t)\, Cos(2\pi f_c t) - S_Q(t)\, Sin(2\pi f_c t) \quad \ldots (1)$$

where, a_i and b_i are the signal amplitudes, while T_s is the symbol interval for the real (i) and imaginary (j) co-ordinates respectively. Further, the signal x(t) modulates the electrical signal and the intensity of the optical source. Hence, the transmitted optical signal current for the modulation index μ is written by

$$S(t) = P_s[1 + \mu x(t)] \quad \ldots (2)$$

The signal received at the receiver end after SIM optical detection is expressed as[15]

$$y = \frac{\eta \alpha P_s}{M} H x^U + w, U \in A\{a, b, c\} \quad \ldots (3)$$

In Eq. (3) P_s and η are the average transmitted optical power/symbol, and the optical to electrical conversion efficiency, respectively while $\mathbf{w} \in \mathbb{R}^N$ is the Additive White Gaussian Noise (AWGN) vector with independent and identically distributed elements $\omega_i \sim \left(0, \frac{N_0}{2}\right)$, i = 1, 2,…,N. Here, N_0 and $H \in R^{M \times N}$ express the double sided Power Spectral Density (PSD) in $\left(\frac{W}{Hz}\right)$ and the fading channel matrix with channel coefficients or gain element h_{ij} (i =1, 2,…, *N*, *j* =1, 2,…,N), respectively between the j^{th} transmit and i^{th} receive apertures respectively. Assuming the strong

atmospheric turbulence conditions and the pointing error impairments, the statistical channel model is represented by Eq. (4) [21]

$$h = h_{at}h_{pe} \quad \text{... (4)}$$

where, h_{at} and h_{pe}, represent the atmospheric turbulence and pointing error components, respectively.

Channel Modelling

Modified Malaga Atmospheric Turbulence Model

The received optical signal comprises of Line-Of-Sight (LOS) component (U_L), the coupled to LOS fading component (U_S^C), and the independent scattering fading contribution (U_S^G), respectively. The U_S^G component is statistically independent from the rest of two other components. The average power of these three factors is given by Eq. (5).

$$\delta=E[|U_L|^2], = 2\varepsilon b_o = E\,[|U_S^C|^2] \text{and } g = E\,[|U_S^G|^2] = 2b_o(1-\varepsilon) \quad \text{... (5)}$$

In addition, the total average power in the scattering components is denoted by $2b_o = E\,[|U_S^C|^2 + |U_S^G|^2]$ while the scattering power coupled to U_L component is given by the parameter $0 \le \varepsilon \le 1$.

In this research work, a more generalized Malaga statistical channel is assumed for the proposed system design. This model characterizes most of the probability distributions models, such as Gamma-Gamma (GG), Log-normal, K-distribution, and negative exponential models, for strong to weak atmospheric turbulent conditions. The different sets of parameters and intensity irradiance variation index $\sigma_R^2 = 1.23C_n^2k^{7/6}L^{11/6}$ for the refractive index structure parameter C_n^2, optical wave number $k = \frac{2\pi}{\lambda}$, transmission link distance L, and optical wavelength λ are given in Table 1.[21]

However, this distribution model is primarily used for strong atmospheric conditions, including pointing errors, and is represented by the Probability Density Function (PDF) of the intensity fluctuations of the received signal h_{at}.[5,12]

Table 1 — Malaga distribution model

Distribution Model	Set of Parameter	$\alpha, \beta, \sigma_R^2$
Lognormal Model	ε=0, δ=1, $b_o \to 0$, $g \to 0$	11, 10, 0.2
GG Model	ε =1, δ = 0.5, b_o=0.25, g=0	8, 3, 0.5
K- Model	$\varepsilon = 0, \delta = 0$, b_o= 0.5	2, 2, 2

$$f_{h_{at}}(h_{at}) = A\sum_{j=1}^{\beta} a_j (h_{at})^{\frac{\alpha+j}{2}-1} . K_{\alpha-j}\left(2\sqrt{\frac{\alpha\beta h_{at}}{g\beta+\delta'}}\right) \quad \text{... (6)}$$

where, A and a_j are defined by Eq. (7)

$$A = \frac{2\alpha^{\frac{\alpha}{2}}}{g^{1+\frac{\alpha}{2}}\Gamma\alpha}\left(\frac{g\beta}{g\beta+\delta}\right)^{\beta+\frac{\alpha}{2}} a_j = \binom{\beta-1}{j-1}\frac{(g\beta+\delta)^{1-\frac{j}{2}}}{(j-1)!}\left(\frac{\delta'}{g}\right)^{j-1}\left(\frac{\alpha}{\beta}\right)^{\frac{j}{2}} \quad \text{... (7)}$$

In the above expressions, K_v (.) and $\mathbb{\Gamma}$ are the 2nd order modified Bessel function, and Gamma function, whereas the average power due to coherent contribution is represented by $\delta' = \delta + 2\varepsilon b_o + 2\sqrt{2b_o\delta_\varepsilon Cos\,(\theta_A - \theta_B)}$ for the deterministic angles (θ_A, θ_B) due to loss and coupled to LOS fading components, respectively.[22] In addition, (α, β) are the scintillation parameters, which define the fluctuation strength of the irradiance of the turbulence. For the comprehensive analytical analysis, the second term in Eq. (6), which specifies the Bessel function, can be modified in terms of the Meijer-G function $\left[G_{p,q}^{m,n}(.)\right]$ assuming $b_j = a_j\left(\frac{\alpha\beta h_{at}}{g\beta+\delta'}\right)^{-\alpha+\frac{j}{2}}$ and stated as[23]

$$f_{h_{at}}(h_{at}) = \frac{A}{2}\sum_{j=1}^{\beta} b_j (h_{at})^{-1} G_{1,2}^{2,0}\left(\frac{\alpha\beta h_{at}}{g\beta+\delta'}\right) \quad \text{... (8)}$$

where, the values of α and β are defined by the Eq. (9) and considered (α = 4.2, β = 1.2) for strong atmospheric turbulence condition.

$$\alpha = \left[e^{\left[\frac{0.49\sigma_R^2}{(1+1.11\sigma_R^{2.4})^{7/6}}\right]-1}\right]^{-1}, \quad \beta = \left[e^{\left[\frac{0.51\sigma_R^2}{(1+0.69\sigma_R^{2.4})^{5/6}}\right]-1}\right]^{-1} \quad \text{... (9)}$$

Pointing Error

Pointing errors, which occur primarily as a result of transmitter and receiver misalignment, play an important role in reliable FSO link performance. The fraction of received power (h_{pe}) in the transverse plane for a circular Gaussian beam profile with radius 'a' is approximated at the receiver end by the pointing error 'r' and stated as[5]

$$h_{pe}(r,z) = A_0 e^{\left(\frac{-2r^2}{w_{zeq}^2}\right)}, \text{ and } \omega_{zeq}^2 = \omega_z^2\frac{\sqrt{\pi}erf\left(\frac{\sqrt{\pi}a}{\sqrt{2}\omega_z}\right)}{2\left(\frac{\sqrt{\pi}a}{\sqrt{2}\omega_z}\right)e^{-\left(\frac{\sqrt{\pi}a}{\sqrt{2}\omega_z}\right)^2}} \quad \text{... (10)}$$

The term $A_0 = \text{erf}(\frac{\sqrt{\pi}a}{\sqrt{2}\omega_z})$ denotes the fraction of the collected power at r = 0 for the error function erf (·), ω_{zeq}^2 is the equivalent beam width, and ω_z is the beam waist radius, respectively. For the displacement standard deviation σ_s at the receiver, and, $g = \frac{\omega_{zeq}}{2\sigma_s}$, PDF of the pointing error impairments (h_{pe}) is defined by[24, 25]

$$f_{h_{pe}}(0 \le h_{pe} \le A_0) = \frac{g^2}{A_0^{g^2}} h_{pe}^{s^2-1} \quad \text{... (11)}$$

The Meijer-G function shown in Eq. (8) adds complexity in analytical designing of the MIMO-OFDM-FSO link. So, a new modified PDF with power series is proposed using the existing Malaga (M) distribution model and pointing error. It not only minimizes the complexity but also improves the diversity gain of the MIMO-OFDM-FSO link. Hence, the term $\left[G_{1,2}^{2,0}(.)\right]$ can further be modified and rewritten as stated in Eq. (12), by assuming $u = \frac{\alpha\beta h_{at}}{g\beta+\delta'}$ and generalizing the hypo-geometric function$_p$ F_q [a_j; b_q; u] respectively.[26]

$$G_{1,2}^{2,0}(u|\alpha, i) = \mathbb{\Gamma}[j-\alpha](u)^{\alpha}{}_{.0}\,F_1[(1+\alpha-j); u] + \mathbb{\Gamma}[\alpha-j](u)^{j}{}_{.0} \times F_1[(1-\alpha+j); u] \quad \text{... (12)}$$

Using Eq. (12), Eq. (8), and Eq. (6), Laplace transforms, the Pochhammer symbol $(\alpha)_k$, and the power series algebra representation shown by Eq. (13), we can derive the modified Malaga distribution in terms of power series representation as follows:

$${}_1F_2[a_1; b_1, b_2.u] = \sum_{k=0}^{\infty} \frac{(a_1)_k u^k}{(b_1)_k (b_2)_k !k} \quad \text{... (13)}$$

$${}_0F_1\left[(1-\alpha+j); \frac{\alpha\beta h_{at}}{g\beta+\delta}\right] = \sum_{k=0}^{\infty} \frac{1}{(1-\alpha+j)_{k!}!k} \left(\frac{\alpha\beta h_{at}}{g\beta+\delta}\right)^k; \times {}_0F_1\left[(1+\alpha-j); \frac{\alpha\beta h_{at}}{g\beta+\delta}\right] = \sum_{k=0}^{\infty} \frac{1}{(1+\alpha-j)_{k!}!k} \left(\frac{\alpha\beta h_{at}}{g\beta+\delta}\right)^k$$

$$f_{h_{at}}(h_{at}) = \sum_{j=1}^{\beta} \sum_{k=0}^{\infty} C_{k1}(\propto, j).(h_{at})^{(k+\propto-1)} + \sum_{j=1}^{\beta} \sum_{k=0}^{\infty} C_{k2}(\propto, j).(h_{at})^{(k-j-1)} \quad \text{... (14)}$$

$$C_{k1}(\alpha, j) = \frac{Ab_j \mathbb{\Gamma}(j-\alpha)}{2(1-\alpha+j)_{k!}} \left(\frac{\alpha\beta h_{at}}{g\beta+\delta}\right)^{k+\alpha}; \text{ and } C_{k2}(\alpha, j) = \frac{Ab_j \mathbb{\Gamma}(a-j)}{2(1-a+j)_{k!}} \left(\frac{\alpha\beta h_{at}}{g\beta+\delta}\right)^{k-j} \quad \text{... (15)}$$

The PDF of $(h_{at})^2$ can be derived using Eq. (15), by changing the variable techniques as follows

$$f_{(h_{at})^2}(h_{at}) = \sum_{j=1}^{\beta} \sum_{k=0}^{\infty} \frac{C_{k1}(\alpha,j)}{2}.(h_{at})^{\frac{k+\alpha}{2}-1} + \sum_{j=1}^{\beta} \sum_{k=0}^{\infty} \frac{C_{k2}(\alpha,j)}{2}.(h_{at})^{\frac{k+j}{2}-1} \quad \text{... (16)}$$

By similar process, the PDF of the pointing error can be also obtained by replacing h_{at} by h_{pe}.[26]

Combined Channel Statistical Model

The composite PDF for both the atmospheric turbulence and pointing error channel impairments can be obtained using Slater theorem the Meijer-G function with Eq. (6) in simplified form by using Eq. (17)

$$f_h(h) = \frac{\alpha\beta\zeta^2}{A_0 \mathbb{\Gamma}\alpha \mathbb{\Gamma}\beta}\left[\mathbb{\Gamma}(\alpha-\zeta^2)\mathbb{\Gamma}(\beta-\zeta^2)\left(\frac{\alpha\beta h}{A_0}\right)^{\zeta^2-1} * 1 + \frac{\mathbb{\Gamma}(-\alpha+\beta)\mathbb{\Gamma}(-\alpha+\zeta^2)}{\left(\mathbb{\Gamma}(1+\zeta^2-\alpha)\right)}\left(\frac{\alpha\beta h}{A_0}\right)^{-1+\alpha} \sum_{m=0}^{\infty} \frac{(\alpha-\zeta^2)_n}{(1+\alpha-\zeta^2)_n (1+\alpha-\beta)_n} \frac{\left(\frac{\alpha\beta h}{A_0}\right)^n}{(n!)} + \frac{\mathbb{\Gamma}\,\mathbb{\Gamma}(-\beta+\zeta^2)}{\mathbb{\Gamma}(1+\zeta^2-\beta)}\left(\frac{\alpha\beta h}{A_0}\right)^{-1+\beta} \sum_{m=0}^{\infty} \frac{(\beta-\zeta^2)_n}{(1+\beta-\zeta^2)_n (1-\alpha+\beta)_n} \frac{\left(\frac{\alpha\beta h}{A_0}\right)^n}{(n!)}\right] \quad \text{… (17)}$$

Applying Eq. (13) to Eq. (17) and using some algebra, we can get the proposed simplified PDF of the composite channel $h = h_{at}h_{pe}$ with only two h-exponents of power series, in which it is easy to calculate the integral calculation as compared to Meijer-G using operational properties in Eq. (12), for $B = \frac{\gamma\beta+\varepsilon}{\alpha\beta}$ as shown below[26]

$$f_h(h) = x_o h^{\zeta^2-1} + \sum_{m=0}^{\infty} y_o h^{n+\alpha-1} + \sum_{m=0}^{\infty} z_o h^{n+\beta-1}$$

$$f_h(h) = \frac{g^2 A h^{-1}}{2}\left(\sum_{k=1}^{B} a_k \left(\frac{1}{B}\right)^{\frac{-\alpha+k}{2}} G_{1,3}^{3,0}\left|\frac{h}{BA_0h_i}\right| \begin{matrix} 1+g^2 \\ g^2, \alpha, \beta \end{matrix}\right) \quad \text{... (18)}$$

Adaptive Switching based MIMO-OFDM-FSOC System Schematic

The schematic design of the proposed MIMO-OFDM-FSOC for transmitter and receiver subsystems systems based on the adaptive switching algorithm are illustrated as Fig. 1 and Fig. 2, respectively. The transmitter section is equipped with four sub-systems, from the data source to the laser drive module, as shown in Fig. 1. The 'k-bit binary data generated at the output of the Pseudo-Random Binary Source (PRBS) is fed to the 'n-bit LDPC linear block encoder with a code rate of r = k/n before modulating it using

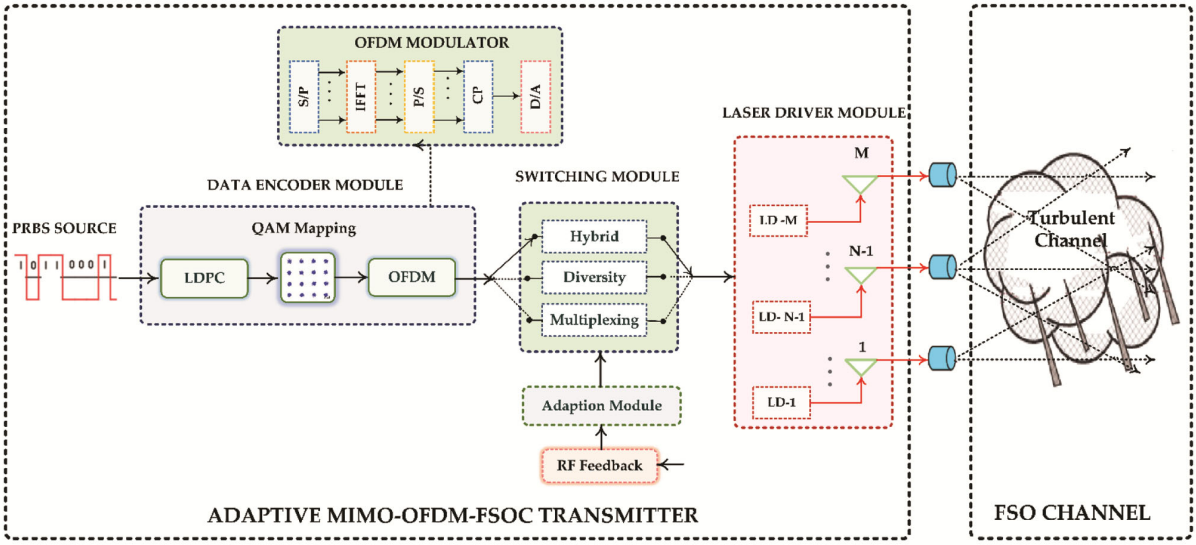

Fig. 1 — Proposed schematic design of the adaptive MIMO-OFDM-FSOC transmitter

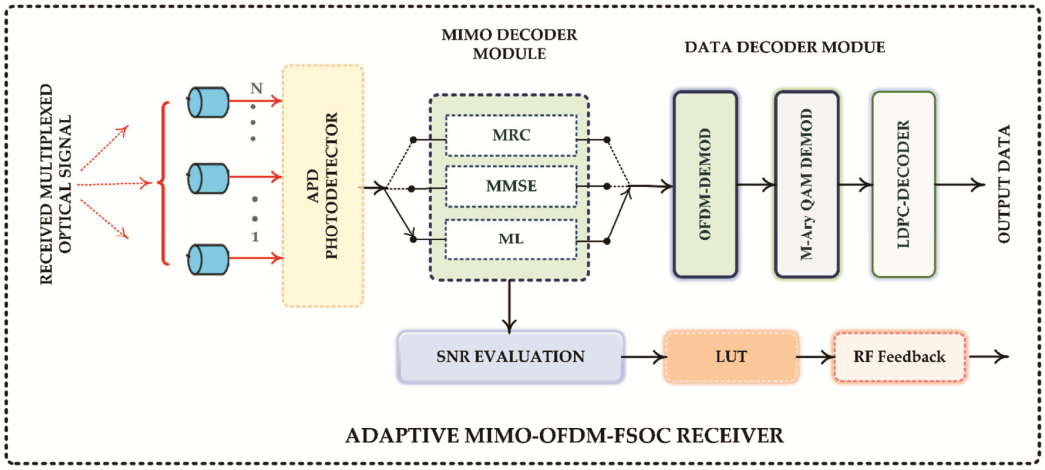

Fig. 2 — Proposed schematic design of the adaptive MIMO-OFDM-FSOC receiver

16-QAM modulation. These LDPC-coded data blocks consist of a minimal number of ones, which are used to minimize the complexity of the computation algorithm for long data blocks. These codes can be efficiently applied to combat fading channels to achieve approximate Shannon channel capacity in a high-speed MIMO system. In our proposed system, the ½ code rate LDPC codes are included to enhance system performance with high coding gain.[27] The 16-QAM-modulated serial LDPC-coded bit streams are then transformed to parallel bit streams based on the number of sub-carriers and laser diodes used in the MIMO-OFDM-FSOC system. In the OFDM section, the IFFT block is used to modulate a QAM modulated bit stream using a sub-carrier, producing a single OFDM symbol. A cyclic prefix is added between the symbols to provide a guard time and reduce carrier interference. The digital-to-analog (D/A) block in the OFDM section is used to convert the parallel binary stream back to an analog signal. This OFDM- coded signal is then fed to the adaptive switching module, where any one of the switching mode is selected based on the received RF feedback signal from the optical receiver. At the receiver, the instantaneous SNR is modified according to the composite atmospheric channel fading conditions and then compared against the threshold SNR values maintained in the LUT. This compared feedback signal is then utilized to select the best adaptive MIMO switching technique at the transmitter's end

through the low rate-RF control link, and the output of the switching module is then sent over the turbulent atmosphere channel using M laser diodes.

In this research paper, MIMO-OFDM-FSOC adaptive system is designed to develop LUTs based on ACC and ABER to optimize the data rate 'R' while satisfying the predetermined outage probability. An outage probability (OP) $P_{out}(R,\gamma_0)$ occurs when the instantaneous channel capacity $C(\mathbf{H})$ falls below the target data rate R. The OP and the instantaneous channel capacity for an average electrical SNR (γ_0) at the receiver are shown by Eq.19 and Eq. 20, respectively.[15,28,29]

$$P_{out}(R,\gamma_0) = P_r\{C(\mathbf{H}) < R\} \quad \text{... (19)}$$

$$\overline{C}^t(\mathbf{H}) = \int_0^\infty C(\mathbf{H}) f_h(h)dh \quad \text{... (20)}$$

$$C(\mathbf{H}) = \frac{1}{2}\log_2\left(\left|I_N + \frac{\gamma_0}{M^2}\mathbf{H}\mathbf{H}^T\right|\right) \quad \text{... (21)}$$

$$\gamma_0 = \frac{2\eta^2 L^2 P_T^2}{N_o} \quad \text{... (22)}$$

Outage capacity $C_\epsilon(\gamma_0)$ is the optimum rate that can be achieved while maintaining the outrage probability $P_{out}(R,\gamma_0) \le \epsilon$(constant) and can be expressed mathematically for a cumulative distribution function (CDF) $F_C(.)$ of C (**H**) by[30]

$$C_\varepsilon(\gamma_0) = \max\{R: P_{out}(R,\gamma_0) \le \varepsilon\} = F_C^{-1}(\varepsilon) \quad \text{... (23)}$$

If $P_{out}^t(R,\gamma_0)$ and $C_\varepsilon^t(\gamma_0)$, for $t \in D$, indicates the outage probability and outage capacity or ACC for the t^{th} switching operation for the D as a set of divisor of M assuming $t = 1$ for diversity while $t = M$ for spatial multiplexing switching operations respectively. Similarly, hybrid switching operation is considered for $t \in D$ and $t \neq 1, t \neq M$. Further, to obtain maximum outage capacity for a particular switching mode, the SNR (γ_0) range is divided into different regions for the selected operation mode ($\hat{t} \in D$) and the design problem and the LUT is constructed using Eq. 24 by determining the threshold points at which one switching operation can be moved to another switching mode operation.

$$\hat{k} = \arg\max_t C_\epsilon^t(\gamma_0) \quad \text{... (24)}$$

Similarly, the corresponding ABER of each data stream for the t^{th} adaptive switching can be calculated for a Gaussian function Q (·) as follows:

$$\overline{ber}^t = \int_0^\infty Q\left(h\sqrt{2\gamma_0}\right) f_h(h)dh \quad \text{... (25)}$$

The maximum value of ACC for the three switching modes is obtained by the appropriate selection of t for the various SNR ranges. The mathematical expressions for the ACC and ABER for various switching modes are discussed in the sections that follow.

Spatial Multiplexing Mode

In this switching mode, each aperture transmits distinct data stream to increase the system throughput for the maximum degree of freedom min (M, N) = M. The simplified diagonal channel matrix for this mode is written by[15]

$$\mathbf{H} = \mathrm{diag}(h_1, h_2, \ldots\ldots\ldots\ldots h_M) \quad \text{... (26)}$$

The instantaneous channel capacity$C(H)$, average channel capacity $\overline{C}^M(H)$, and the average BER $\overline{ber}^t$ and the total average BER $\overline{ber^M}$ for each data stream in spatial multiplexing switching can be derived using Eqs (18), (20), (21), and operational properties of Meijer G-function and approximation $Q(x) \sim \frac{1}{2}e^{\left(\frac{-x^2}{2}\right)} + \frac{1}{2}e^{\left(\frac{-2x^2}{3}\right)}$as shown below[31,32]

$$C(\mathbf{H}) = \frac{1}{2}\sum_0^\infty \log_2\left(1 + \frac{\gamma_0}{M^2}|h_j|^2\right) \quad \text{... (27)}$$

$$\overline{C}^M(\mathbf{H}) = \frac{M2^\alpha gA}{32\pi \ln 2}\left[\frac{1}{B}\right]^{\frac{-\alpha}{2}}\sum_{k=1}^{\beta} a_k\left[\frac{1}{B}\right]^{\frac{-k}{2}} 2^k G_{8,4}^{1,8} \times\left(\frac{\gamma_0}{M^2}16\beta^2 A_0^2 h_{ll}^2\middle| 1,1,\frac{1-g^2}{2},\frac{2-g^2}{2},\frac{1-\alpha}{2},\frac{2-\alpha}{2},\frac{1-k}{2},\frac{2-k}{2},\frac{-g^2}{2},\frac{1-g^2}{2}\right) \quad \text{... (28)}$$

$$\overline{ber}^t = \frac{1}{12}\int_0^\infty e^{(-\gamma_0 h^2)} f_h(h)dh + \frac{1}{4}\int_0^\infty e^{\left(-\frac{4\gamma_0 h^2}{3}\right)} f_h(h)dh \quad \text{... (29)}$$

where, $e^{(-x)} = \left|G_{0,1}^{1,0}[x|_0\right]$

$$\overline{ber(t)} = \frac{g^2 A}{64\pi}\left[\frac{1}{3}\sum_{k=1}^{\beta} a_k\left[\frac{1}{B}\right]^{\frac{-\alpha+k}{2}} 2^{\alpha+k} G_{6,3}^{1,6}\tau + \sum_{k=1}^{\beta} a_k\left[\frac{1}{B}\right]^{\frac{-\alpha+k}{2}} 2^{\alpha+k} G_{6,3}^{1,6}\left\{\frac{4}{3}\tau\right\}\right] \quad \text{... (30)}$$

where, $\tau = \left(h_{ll}^2\gamma_0 B^2 h_{ll}^2 16\middle|\begin{matrix}\frac{1-g^2}{2},\frac{2-g^2}{2},\frac{1-\alpha}{2},\frac{2-\alpha}{2},\frac{1-k}{2},\frac{2-k}{2}\\ 0,\frac{-g^2}{2},\frac{1-g^2}{2}\end{matrix}\right)$

$$\overline{ber^M} = 1 - \prod_{t=1}^{M}(1 - \overline{ber(t)}) \quad \text{... (31)}$$

Diversity Switching Mode

In this switching mode, each aperture transmits a dependent data stream to minimize the effects of multipath channel fading and increase system

performance. For this switching mode, we can rewrite Eq. 3 for the channel matrix **H** as shown below[15]

$$y_i = \frac{\eta}{M}\left(\sum_{j=1}^{M} h_{ij}\right)x_i^B + w_i i=1,\ 2\ldots\ldots..N \quad \ldots (32)$$

$$\mathbf{H} = \begin{bmatrix} h_{11} & \cdots & h_{1j} \\ \vdots & \ddots & \vdots \\ h_{i1} & \cdots & h_{ij} \end{bmatrix}$$

Also, substituting Eq. (26) into Eq. (21), we can obtain the instantaneous channel capacity while the average channel capacity for the diversity switching is obtained using Eqs (18), (20), and (33), respectively and expressed by Eq. (34)

$$C(\boldsymbol{H}) = \frac{1}{2} log_2\left[1 + \frac{\gamma_0}{M^2}\sum_{i=1}^{N}\left(\sum_{j=1}^{M} h_{ij}\right)^2\right] \quad \ldots (33)$$

$$\bar{C}^1(\mathbf{H}) = \int_0^\infty \frac{1}{2}\log_2\left(1 + \frac{\gamma_0}{M^2}\sum_{i=1}^{N}\left(\sum_{j=1}^{M} h_{ij}\right)^2\right)\frac{g^2 A h^{-1}}{2}\sum_{k=1}^{\beta}\left(a_k\left[\frac{1}{B}\right]^{-\frac{\alpha+k}{2}} G_{1,3}^{3,0}\left(\frac{h}{BA_0 h_i}\Big|_{g^2,\alpha,k}^{1+g^2}\right)\right)dh = \frac{g^2 A}{4\ln 2}\sum_{k=1}^{\beta} a_k\left[\frac{1}{B}\right]^{-\frac{\alpha+k}{2}}\int_0^\infty h^{-1}\ln(1 + \gamma_0 N h^2) G_{1,3}^{3,0}\left(\frac{h}{BA_0 h_l}\Big|_{g^2,\alpha,k}^{1+g^2}\right)dh \quad \ldots (34)$$

Using properties of Meijer G-function[32], Eq. (34) can be transformed into:

$$\bar{C}^1(\mathbf{H}) = \frac{2^\alpha g^2 A}{32\pi\ln 2}\left[\frac{1}{B}\right]^{-\frac{\alpha}{2}}\sum_{k=1}^{\beta} a_k\left[\frac{1}{B}\right]^{-\frac{k}{2}} 2^k \times G_{8,4}^{1,8}\left(16\gamma_0 N B^2 A_0^2 h_l^2 \times \begin{matrix} 1,1,\frac{1-g^2}{2},\frac{2-g^2}{2},\frac{1-\alpha}{2},\frac{2-\alpha}{2},\frac{1-k}{2},\frac{2-k}{2} \\ 1,0,\frac{-g^2}{2},\frac{1-g^2}{2} \end{matrix}\right) \quad \ldots (35)$$

The average BER of this mode is determined using Eq. (35), assuming equal gain combining (EGC) at the receiver, whereas the estimated closed-form for ABER can be deduced by arranging Eqs (25) and utilizing the Meijer G-function property.[32]

$$\overline{BER}^1 = \int_0^\infty Q\left(\sqrt{\frac{2\gamma_0}{MN}}\sum_{i=1}^{N}\sum_{j=1}^{M} h_{ij}\right) f_{h_{ij}}(h_{ij})dh_{ij} = \frac{1}{12}\prod_{i=1}^{N}\prod_{j=1}^{M}\int_0^\infty f_{h_{ij}}(h_{ij}) G_{0,1}^{1,0}\left[\frac{\gamma_0 h_{ij}^2}{MN}\Big|_0\right] dh_{ij} + \frac{1}{4}\prod_{i=1}^{N}\prod_{j=1}^{M}\int_0^\infty f_{h_{ij}}(h_{ij}) G_{0,1}^{1,0}\left[\frac{4\gamma_0 h_{ij}^2}{3MN}\Big|_0\right] dh_{ij} \quad \ldots (36)$$

Hybrid Switching Mode

The diversity and spatial multiplexing switching modes are combined to obtain hybrid switching mode by constructing t parallel data streams through M transmit apertures. In this mode, repeat codes are sent over $\left(\frac{M}{t}\right)$ different apertures and M is multiples $of\, t$. The i[th] received signal at the l[th] data stream can be represented by Eq. (37)

$$y_{i,l} = \frac{\eta}{M}\left(\sum_{j=1}^{M/t} h_{ij}^l\right)x_l^C + w_{i,l} \text{ for } i = 1,\ldots,\frac{N}{t}, l = 1,\ldots,t \quad \ldots (37)$$

where, h_{ij}^l is the channel coefficient from the j^{th} transmit aperture to the i^{th} receive aperture in the l^{th} data stream. For this mode, the channel matrix **H** is denoted by Eq. (38), and the instantaneous channel capacity can be derived by substituting Eq. (21) in Eq. (38)

$$\boldsymbol{H} = \begin{bmatrix} h_{11}^1 + h_{12}^1 + \cdots + h_{1j}^1 & \cdots & 0 \\ \vdots & \ddots & \vdots \\ 0 & \cdots & 0\ldots.\ 0\ h_{i1}^l + h_{i2}^l + \cdots + h_{ij}^l \end{bmatrix}_{N\times t} \quad \ldots (38)$$

$$C(\boldsymbol{H}) = \frac{1}{2}\sum_{l=1}^{t}\log_2\left(1 + \frac{\gamma_0}{M^2}\sum_{i=1}^{N/t}\left(\sum_{j=1}^{M/t} h_{ij}^l\right)^2\right) \quad \ldots (39)$$

The simplified form of the average channel capacity of this hybrid switching mode is shown in Eq. (41), which is derived by using Eqs (20), (21), (39) and the Meijer G-function property, respectively.[32]

$$\bar{C}^t(\mathbf{H}) = \int_0^\infty \frac{1}{2}\sum_{l=1}^{t}\log_2\left(1 + \frac{\gamma_0}{M^2}\sum_{i=1}^{N/t}\left(\sum_{j=1}^{M/t} h_{ij}^l\right)^2\right)\frac{g^2 A h^{-1}}{2}\sum_{k=1}^{\beta}\left(a_k\left[\frac{1}{B}\right]^{-\frac{\alpha+k}{2}} G_{1,3}^{3,0}\left(\frac{h}{BA_0 h_l}\Big|_{g^2,\alpha,k}^{1+g^2}\right)\right)dh = \frac{g^2 At}{4\ln 2}\sum_{k=1}^{\beta} a_k\left[\frac{1}{B}\right]^{-\frac{\alpha+k}{2}}\int_0^\infty h^{-1}\ln\left(1 + \frac{\gamma_0}{M^2}\frac{N}{t}\left(\frac{M}{t}h\right)^2\right) G_{1,3}^{3,0}\left(\frac{h}{BA_0 h_l}\Big|_{g^2,\alpha,k}^{1+g^2}\right)dh \quad \ldots (40)$$

$$\bar{C}^t(\mathbf{H}) = \frac{Ag^2 t}{32\pi\ln 2} 2^\alpha\left[\frac{1}{B}\right]^{-\frac{\alpha}{2}}\sum_{k=1}^{\beta} a_k\left[\frac{1}{B}\right]^{-\frac{k}{2}} 2^k \times G_{8,4}^{1,8}\left(\frac{\gamma_0 N}{t^3} 16 B^2 A_0^2 h_l^2 \times \begin{matrix} 1,1,\frac{1-g^2}{2},\frac{2-g^2}{2},\frac{1-\alpha}{2},\frac{2-\alpha}{2},\frac{1-k}{2},\frac{2-k}{2} \\ 1,0,\frac{-g^2}{2},\frac{1-g^2}{2} \end{matrix}\right) \quad \ldots (41)$$

Moreover, the ABER of the l^{th} data stream can be derived using Eq. (42) and expressed as Eq. (43) as follows:

$$\overline{BER(l)} = \int_0^{\infty} Q\left(\frac{\sqrt{2\gamma_0}}{MN/t^2}\sum_{i=1}^{N/t}\sum_{j=1}^{M/t} h_{ij}\right) f_{h_{ij}}(h_{ij})dh_{ij}$$
$$= \frac{1}{12}\prod_{i=1}^{N}\prod_{j=1}^{M}\int_0^{\infty} f_{h_{ij}}(h_{ij})G_{0,1}^{1,0}\left[\frac{\gamma_0 t^2 h_{ij}^2}{MN}\Big|_0\right]dh_{ij}$$
$$+\frac{1}{4}\prod_{i=1}^{N}\prod_{j=1}^{M}\int_0^{\infty} f_{h_{ij}}(h_{ij})G_{0,1}^{1,0}\left[\frac{4\gamma_0 t^2 h_{ij}^2}{3MN}\Big|_0\right]dh_{ij} \quad \ldots (42)$$

$$\overline{BER(l)} = \prod_{i=1}^{N/t}\prod_{j=1}^{M/t}\frac{g^2 A}{64\pi}\sum_{k=1}^{\beta} a_k\left[\frac{1}{B}\right]^{-\frac{\alpha+k}{2}} 2^{\alpha+k} G_{6,3}^{1,6}\left(\frac{\gamma_0 t^2}{MN}B^2 A_0^2 h_l^2 16\right)\times$$
$$\left[\frac{1}{3}\left|\begin{matrix}\frac{1-g^2}{2},\frac{2-g^2}{2},\frac{1-\alpha}{2},\frac{2-\alpha}{2},\frac{1-k}{2},\frac{2-k}{2}\\ 0,\frac{g^2}{2},\frac{1-g^2}{2}\end{matrix}\right. + \frac{4}{3}\left|\begin{matrix}\frac{1-g^2}{2},\frac{2-g^2}{2},\frac{1-\alpha}{2},\frac{2-\alpha}{2},\frac{1-k}{2},\frac{2-k}{2}\\ 0,\frac{-g^2}{2},\frac{1-g^2}{2}\end{matrix}\right.\right] \quad \ldots (43)$$

On the hand, the total ABER for the hybrid switching mode is derived by using the same process as used for diversity and multiplexing mode and can be expressed by Eq. (44).

$$\overline{BER}^t = 1 - \prod_{l=1}^{t}(1 - \overline{BER(l)}) \quad \ldots (44)$$

Results Discussions

In this work, the performance of the MIMO-OFDM-FSOC based on the adaptive switching algorithm is investigated under the composite atmospheric turbulent FSO channel. The 16-QAM modulation and LDPC channel coding techniques are also incorporated into the proposed system to mitigate atmospheric turbulence and hence improve the system's performance. Furthermore, the atmospheric channel comprises a power series-based modified Malaga distribution considering strong atmospheric turbulence ($c_n^2 = 7 \times 10^{-14} m^{-2/3}$) and the pointing error derived in the previous section. This section also constructs LUTs for the three different adaptive switching algorithms and investigates their performance for metrics such as outage channel capacity and average BER under moderately clear sky with an attenuation constant of α = 0.75 dB/km, and for a assumed link a distance of 1 km, respectively. The proposed system and atmospheric link parameters are also summarized in Table 2.

The simulated plots between the outage capacities vs. different SNR for the multiple apertures (4×4 and 6×6) MIMO-OFDM-FSOC system based on adaptive switching algorithms are illustrated in Fig. 3(a) and Fig. 3(b), respectively, considering a targeted outage of $\epsilon = 0.1$ for the three distinct switching algorithms: spatial multiplexing, diversity, and hybrid algorithms

Table 2 — Proposed system simulation parameters[11]

Parameter	Symbols	Values
MIMO aperture configuration	M × N	4 × 4, 6 × 6
Laser wavelength	λ	1550 nm
Maximum bit Rate	R	10 Gb/s
LDPC code rate	k	½
Modulation	m	16
Modulation index	μ	1
No of data sub-carriers	N_D	110
No of pilot sub-carriers	N_p	18
No. of sub-carriers	N_{sub}	128
Efficiency of photodiode	η	0.75
Photodiode responsivity	R	0.9 A/m
Receiver aperture diameter	d_r	10 cm
Beam divergence angle	θ_{tx}	1 mrad
Dark current	I_o	10 nA
Atmospheric link parameters		
Refractive-index structure constant	C_n^2	7×10^{-14} $m^{-2/3}$
Rytov variance	σ_{lnh}^2	0.22
Visibility range	V	10 km
Link distance	L	1 km
Noise power density	N_o	10^{-4} W/Hz

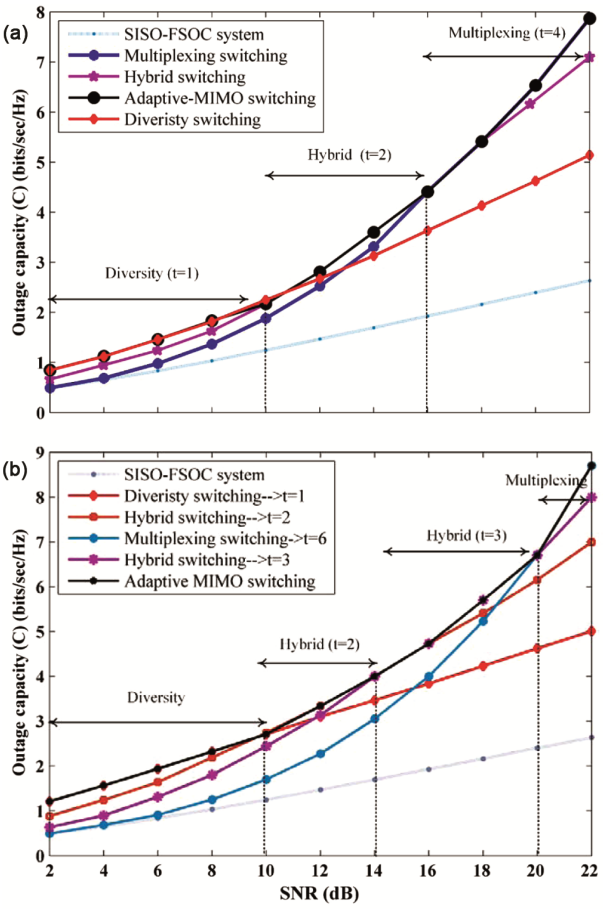

Fig. 3(a) — Outage capacity of 4 × 4 MIMO-OFDM-FSOC adaptive system; and (b) Outage capacity of 6 × 6 MIMO-OFDM-FSOC adaptive system

in the K-distribution FSO channel. The outage capacity of the three adaptive switching algorithms-based MIMO-OFDM-FSOC systems is compared to that of the SISO-FSOC system, which is considered to be the reference point. As shown in Fig. 3 (a), value of $t = 4$ is set for the spatial multiplexing switching to transmit the four distinct data streams in parallel, while $t = 2$ is fixed for the hybrid switching for the two different repetition codes, which run in parallel for the 4 × 4 MIMO aperture configuration. The outage capacity for the three different switching operations is obtained from the equations derived in the previous channel modelling section. Also, a LUT is constructed using Eq. 24 for the targeted outage $\epsilon = 0.1$, which specifies the different SNR regions corresponding to each switching mode and is shown in Table 3. The result obtained in Fig. 3 clearly depicts the performance of the adaptive switching algorithm based on the three switching operations, in which a unique switching mode is chosen to obtain the highest possible outage capacity corresponding to each SNR region. For the SNR region of $\gamma_0 \leq 10$ dB, the proposed adaptive switching selects the diversity switching ($t = 1$) to achieve the highest outage capacity rate under the worst channel conditions, whereas for the SNR region of 10 dB $\leq \gamma_0 \leq$ 16 dB, the adaptive switching system adapts the hybrid switching ($t = 2$) to ensure a trade-off between link reliability and the data rate. Finally, for the SNR region beyond the SNR range of $\gamma_0 \geq 16$ dB, the spatial multiplexed switching scheme must be selected to achieve the highest outage capacity or data rate.

Similarly, the outage capacity for different SNR ranges of the various switching modes is illustrated in Fig. 3(b) for the 6 × 6 MIMO aperture configuration of the proposed adaptive system by keeping the same values of targeted outage of $\varepsilon = 0.1$ and link distance of 1 km. Further, the number of data streams for $t = 1$ corresponds to the diversity switching scheme, whereas $t = 6$ is used for the spatial multiplexing switching scheme. However, for hybrid switching modes, we have considered two sets $t = 2$ and $t = 3$. A LUT is also constructed for this MIMO configuration as given in Table 3. The result obtained in Fig. 3 (b) clearly indicates that for SNR region of $\gamma_0 < 9.99$ dB, diversity switching ($t = 1$) is adopted, whereas hybrid switching mode is selected for the two values of $t = 2$ and $t = 3$ for the SNR range lying between 9.99 dB $< \gamma_0<$ 20.02 dB, respectively. Finally, beyond the SNR range of $\gamma_0 > 20.02$ dB, the spatial multiplexing switching mode ($t = 6$) is preferred to transmit the data streams.

In line with the results presented in Fig. 3(a) and Fig. 3(b), it is observed that a higher MIMO aperture configuration (6 × 6) is more flexible and provides a more numbers of SNR regions for different switching modes. For the hybrid switching operation, it offers two different SNR regions back to back corresponding to values $t = 2$ and $t = 3$, respectively. The diversity switching mode, adopted by the 4×4 aperture configuration gives SNR of $\gamma_0 < 10$ dB whereas this SNR value reduces slightly to SNR value of $\gamma_0 < 9.99$ dB, respectively. As expected, a higher data rate or outage capacity (2.95 bits/sec/Hz) is achieved for the 6 × 6 MIMO aperture configuration as compared to 6 × 6 configuration (2.25 bits/sec/Hz). At SNR = 22 dB, a 6 × 6 MIMO system may obtain a maximum data rate of 8.85 bits/s/Hz, whereas a 4 × 4 MIMO system can achieve 7.93 bits/s/Hz under spatial multiplexing switching operation.

The average BER vs. SNR performance of the proposed 4 × 4 MIMO-OFDM-FSOC system for different pointing error constants (w_z and σ_s) under K- distribution are demonstrated in Fig. 4(a) and Fig. 4(b), respectively. The simulated plots clearly showed that ABER in both of these cases is $\leq 10^{-1}$ during the transition of each switching operation. When the pointing error constants $\frac{w_z}{a}$ and $\frac{\sigma_z}{a}$ are changed from $10 \rightarrow 5$ and $1.5 \rightarrow 2$, respectively, the SNR required for diversity switching is also changed from 27.8 dB → 24.9 dB which means the diversity switching requires almost 2.9 dB less threshold SNR for almost the same ABER performance of 10^{-3}. On the other hand, switching from hybrid to spatial multiplexing transition requires almost 5.3 dB less threshold SNR for the same ABER performance of 10^{-1}, even though the changes in pointing error constants are the same. This clearly indicates that the parameter w_z has more impact on signal transmission as compared to the parameter σ_s. The result also predicts that diversity switching is always preferred for the lower range of SNR whereas; spatial switching is adopted for the higher range of SNR. However, the

Table 3 — LUTs for MIMO-OFDM-FSOC System (L = 1 km, $\varepsilon = 0.1$, $\frac{w_z}{a} = 10$, $\frac{\sigma_s}{a} = 1.5$)

Switching mode	Diversity ($t = 1$)	Hybrid ($t = 2$)	Hybrid ($t = 3$)	Multiplexing ($t = 4$)
4 × 4	$\gamma_0 < 10$ dB	10 dB $< \gamma_0 <$ 16 dB	—	$\gamma_0 >$ 16 dB
6 × 6	$\gamma_0 < 9.99$ dB	9.99 dB $< \gamma_0 <$ 14.02 dB	14.02 dB $< \gamma_0 <$ 20.03 dB	$\gamma_0 >$ 20.03 dB

ABER performance is best for spatial multiplexing switching for fixed low SNR threshold.

The impact of the change in the transmitted beam divergence is observed on the outage capacity vs. transmitted power graph as illustrated in Fig. 5 for

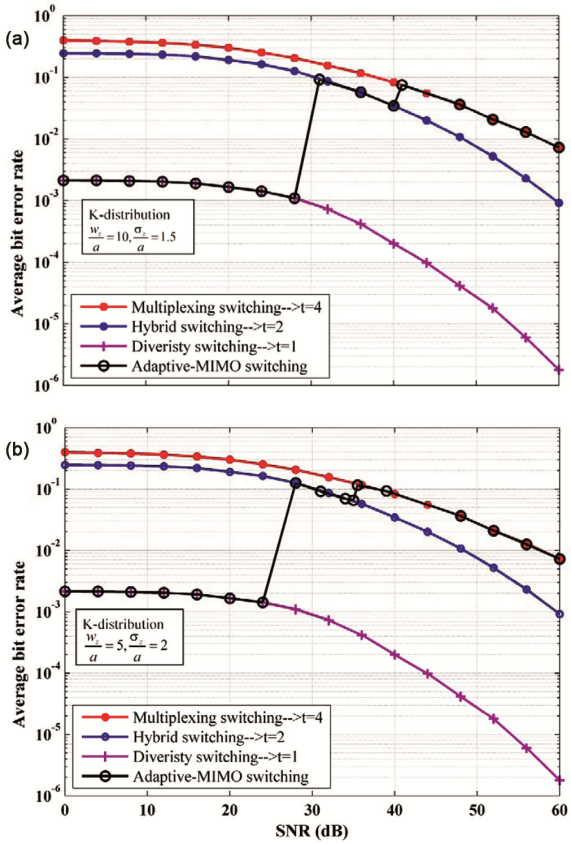

Fig. 4 — (a) Average BER of 4 ×4 MIMO apertures configuration for $\frac{w_z}{a}=10, \frac{\sigma_z}{a}=1.5$ under K- distribution; and (b) Average BER of 4 × 4 MIMO apertures configuration for $\frac{w_z}{a}=5, \frac{\sigma_z}{a}=2$ under K- distribution

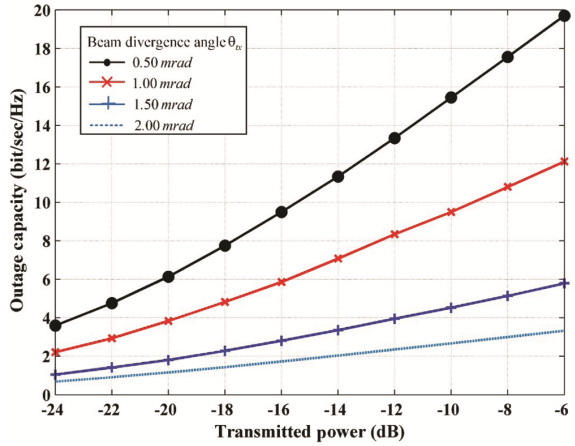

Fig. 5 — Outage capacity vs. transmitted power of 4 ×4 MIMO-OFDM-FSOC adaptive system

4×4 MIMO-OFDM-FSOC system over a link distance of 1 km. The outage capacity increases exponentially with the increase in transmitted power from −24 dB to −6 dB. Keeping the fixed transmitted power of −10 dB, the outage capacity increases from 2.8 bits/sec/Hz to 17.6 bits/sec/Hz with the change in beam divergence angle from 2 mrad to 0.50 mrad. The maximum outage capacity rate is achieved at 20 bits/sec/Hz at −6 dB for a beam divergence angle of 0.5 mrad. Consequently, the results clearly indicate that the outage capacity increases with the minimum power loss when the ample transmitted power is received by the receiver aperture for a narrow divergence angle (0.50 mrad).

Conclusions

In this research paper, we incorporate different adaptive transmission switching techniques such as diversity, hybrid, and spatial multiplexing in the proposed MIMO-FSOC system. The three modes: diversity, multiplexing, and hybrid mode can be selected to transmit the information according to dynamic composite turbulent channel conditions. The OFDM technique is included in the proposed system to minimize the fading effect and enhance its capacity under strong turbulence conditions. The channel is comprised of strong atmospheric turbulence, pointing error, and fixed channel path loss. The Meijer-G function is simplified using a power series technique to formulate a new Probability Density Function (PDF) for the Malaga distribution and pointing error. This derived PDF is used to figure out the maximum outage capacity and average BER needed to meet the target outage probability. It is also used to build a LUT based on the simulation results for each adaptive switching mechanism. The approximated closed-form expression of the average channel capacity and average BER for each operation mode are also derived respectively. Based on the numerical results, a LUT is also constructed under different scenarios to maximize the data rate throughput with a reliable bit error rate. The received SNR is then compared with respect to the threshold SNR listed in the constructed LUT to select the optimal adaptive switching mode. The simulation results revealed that the proposed design of an adaptive FSOC system offers a significant improvement for a spatial multiplexing scheme and that it is a robust scheme as compared to the rest of the proposed transmission schemes. Based on the simulations, it was found that the most reliable data rate is reached for spatial multiplexing only

within a certain range of SNR compared to fixed mode transmission.

Hence, we can conclude that the proposed design is suitable for sub-carrier intensity-based Single Input and Multiple Output (SIMO) and MIMO FSO link, which are widely used for next-generation wireless optical networks. For future work, we can also analyze the proposed system performance under Gamma-Gamma and Log normal distribution. Apart from LDPC channel coding, we can also include other channel coding schemes and higher- order modulation schemes to analyze the system performance.

References

1 Jahid A, Alsharif M & Hall T J, A contemporary survey on free space optical communication: Potentials, technical challenges, recent advances and research direction, *J Netw Comput Appl*, **200** (2022) 103311, doi: https://doi.org/10.1016/j.jnca.2021.103311.

2 Al-Gailani S A, Salleh M F M, Saleem A A, Sahddad R Q, Sheikh U U, Al Gilani A A and Almohamad T A, A survey of free space optics (FSO) communication systems, links and networks, *IEEE Access*, **9** (2021) 7353–73, doi: 10.1109/ACCESS.2020.3048049.

3 Kaushal H & Kaddoum G, Optical communication in space: challenges and mitigation techniques, *IEEE Commun Surv Tutorials*, **19(1)** (2017) 57–96.

4 Balaji K A & Prabu K, MIMO–OFDM free space optical communication system with low-density parity-check code evaluation of FSO system using wavelength and time diversity over Malaga turbulence channel with pointing errors, *Opt Commun*, **410** (2018) 643–651, doi: 10.1016/j.optcom.2017.11.006.

5 Navas A J, Balsells J M G, Paris J F & Notario A P, A unifying statistical model for atmospheric optical scintillation, *Numer Simul Phys Eng Process*, **181(8)** (2011) 181–205.

6 Peppas K P & Datsikas C K, Average symbol error probability of general-order rectangular quadrature amplitude modulation of optical wireless communication systems over atmospheric turbulence channels, *J Opt Commun Netw*, **2(2)** (2010) 102–110, doi: 10.1364/jocn.2.000102.

7 Bhanja U & Panda C, Performance analysis of hybrid SAC-OCDMA-OFDM model over free space optical communication, *CCF Trans Networking*, **3(4)** (2020) 272–85, doi: 10.1007/s42045-020-00039-6.

8 Hasan S M A, Ahmed S & Islam A K M, Simulation of a massive MIMO FSO system under atmospheric turbulence, *5th Int Conf Electr Eng Inform Commun Technol* (Dhaka, Bangladesh) 2021, 1–6.

9 Ai D H, Trung H D & Taun D T, Pointing error effects on performance of amplify-and-forward relaying MIMO/FSO systems using SC-QAM signals over lognormal atmospheric turbulence channels, in *Intelligent Information and Database Systems: 8th Asian Conference,* (Da Nang, Vietnam) 14–16 March 2016.

10 Liu X, Wang P, Liu T, Li Y, Guo L & Tian H, ABER performance of LDPC-coded OFDM free-space optical communication system over exponentiated Weibull fading channels with pointing errors, *IEEE Photon J*, **9(4)** (2017), 1–13, doi: 10.1109/jphot.2017. 2723427.

11 Sharma M, Chadha D & Chandra V, Performance analysis of MIMO–OFDM free space optical communication system with low-density parity-check code, *Photonic Netw Commun*, **32(1)** (2016) 104–114, doi: 10.1007/s11107-015-0579-y.

12 Das A, Bag B, Bose C & Chandra A, Free space optical links over Málaga turbulence channels with transmit and receive diversity, *Opt Commun*, **(456)** (2020) 124591 , doi: 10.1016/j.optcom.2019.124591.

13 Chatzidiamantis N D, Lioumpas A S, Karagiannidis A G K & Arnon S, Adaptive subcarrier PSK intensity modulation in free space optical systems, *IEEE Trans Commun*, **59(5)** (2011) 1368–1377.

14 Garg A, Bhatnagar M R, Berder O & Vrigneau B, Imperfect quantized-feedback-based beamforming for an FSO MISO system over Gamma-Gamma fading with pointing errors, *J Opt Commun Netw*, **9(11)** (2017) 1005–1018.

15 Nouri H & Uysal M, Adaptive MIMO FSO communication systems with spatial mode switching, *IEEE J Opt Commun Netw*, **10(8)** (2018) 686–694.

16 McKay M R, Collings I B, Forenza & Heath R W, Multiplexing/ beamforming switching for coded-MIMO in spatially correlated Rayleigh channels, *IEEE Trans Veh Technol*, **56(5)** (2007) 2555–2567.

17 Heath R W & Paulraj A J, Switching between spatial multiplexing and transmit diversity based on constellation distance, *IEEE Trans Commun*, **53(6)** (2005) 962–968, doi: 10.1109/TCOMM.2005.849774.

18 Karimi M & Uysal M, Novel adaptive transmission algorithms for free-space optical links, *IEEE Trans Commun*, **60(12)** (2012) 3808–3815.

19 Hassan I J, Hossain M J & Cheng J, Performance of MIMO adaptive subcarrier QAM intensity modulation in gamma-gamma turbulence, in *13th Canadian Workshop on Information Theory* (Toronto, Ontario) 2016, 195–199.

20 Safari M & Uysal M, Do we really need OSTBCS for free space optical communication with direct detection?, *IEEE Trans Wireless Commun*, **7(11)** (2008) 4445–4448.

21 Chen D, Liu Y & Wang M, Channel capacity and outage probability analysis for free space optical communication over composite channel, *Opt Rev*, **28(4)** (2021) 368–375.

22 Balaji K A & Prabu K, Performance evaluation of FSO system using wavelength and time diversity over Malaga turbulence channel with pointing errors, *Opt Commun*, **410** (2018) 643–651, doi: 10.1016/j.optcom.2017.11.006.

23 Khan A N, Saeed S, Naeem Y, Zubair M, Massoud Y & Younis U, Atmospheric turbulence and fog attenuation effects in controlled environment FSO communication links, *IEEE Photon Technol Lett*, **34(24)** (2022), 1341–1344, doi: 10.1109/LPT.2022. 3217072.

24 Navas A J, Balsells J M G, Paris J F, Vazquez M C & Notario A P, Impact of pointing errors on the performance of generalized atmospheric optical channels, *Opt Exp*, **20(11)** (2012) 12550–12562.

25 Sandalidis H G, Tsiftsis T A & Karagiannidis G K, Optical wireless communications with heterodyne detection over turbulence channels with pointing errors, *J Light Technol*, **27(20)** (2009) 4440–4445.

26 Bhatnagar M R, A one bit feedback based beam forming scheme for FSO MISO system over gamma-gamma fading,

IEEE Trans Commun, **63(4)** (2015) 1306–1318, doi: 10.1109/tcomm.2015.2391178.

27 Barua B & Barua D, Evaluate the performance of a LDPC coded FSO system employing Q-PPM as modulation, *ACSIT Int J Eng Technol*, **3(3)** (2011) 249–253.

28 Jagadeesh V K, Palliyembil, Muthuchidambaranathan P & Bui F M, Channel capacity and outage probability analysis of sub carrier intensity modulated BPSK system over M-distribution free space optical channel, *Proc IEEE 2nd Int Conf Electron Commun Syst*, 2015, 1051–1054.

29 Samimi P A H, Performance analysis of adaptive subcarrier intensity modulated free-space optical systems, *IET Optoelectron*, **5(4)** (2011) 168–174.

30 Tse S & Viswanath P, *Fundamentals of Wireless Communication* (Cambridge University) 2005.

31 Chiani M, Dardari D & Simon M K, New exponential bounds and approximations for the computation of error probability in fading channels, *IEEE Trans Wireless Commun*, **2(4)** (2003) 840–845.

32 W Research, The mathematical functions site, 2008. [Online]. Available: http://functions.wolfarm.com.